**Atmospheric
Chemistry
and Physics
Discussions**

Physical and optical properties of 2010 Eyjafjallajökull volcanic eruption aerosol: ground-based, LIDAR and airborne measurements in France

M. Hervo[1], B. Quennehen[1], N. I. Kristiansen[3], J. Boulon[1], A. Stohl[3], P. Fréville[1], J. M. Pichon[1], D. Picard[1], P. Labazuy[2], M. Gouhier[2], A. Colomb[1], A. Schwarzenboeck[1], and K. Sellegri[1]

[1]Laboratoire de Météorologie Physique, Observatoire de Physique du Globe de Clermont-Ferrand, Université Blaise Pascal, CNRS UMR6016 – 24 avenue des Landais, 63177 Aubière cedex, France
[2]Laboratoire Magma et Volcan, Observatoire de Physique du Globe de Clermont-Ferrand, Université Blaise Pascal, CNRS, Clermont-Ferrand, France
[3]Norwegian Institute for Air Research, Kjeller, Norway

Title Page

Abstract	Introduction
Conclusions	References
Tables	Figures

|◄ | ►|
◄ | ►

Back | Close

Full Screen / Esc

Printer-friendly Version

Interactive Discussion

Abstract

During the Eyjafjallajökull eruption (14 April to 24 May 2010), the volcanic aerosol cloud was observed across Europe by several airborne in-situ and ground-based remote-sensing instruments. On 18 and 19 May, layers of depolarizing particles (i.e. non-spherical particles) were detected in the free troposphere above the Puy de Dôme station, (France) with a Rayleigh-Mie LIDAR emitting at a wavelength of 355 nm, with parallel and crossed polarization channels. These layers in the free troposphere (FT) were also well captured by simulations with the Lagrangian particle dispersion model FLEXPART, which furthermore showed that the ash was eventually entrained into the planetary boundary layer (PBL). Indeed, the ash cloud was then detected and characterized with a comprehensive set of in-situ instruments at the Puy de Dôme station (PdD). In agreement with the FLEXPART simulation, up to $65\,\mu g\,m^{-3}$ of particle mass and 2.2 ppb of SO_2 were measured at PdD, corresponding to concentrations higher than the 95 percentile of 2 years of measurements at PdD. Moreover, the number concentration of particles increased to $24\,000\,cm^{-3}$, mainly in the submicronic mode, but a supermicronic mode was also detected at 2 µm. The resulting optical properties of the ash aerosol were characterized by a low Ångström exponent (1.1), showing the dominance of supermicronic particles. For the first time to our knowledge, the combination of in-situ optical and physical characterization of the volcanic ash allowed the calculation of the mass-to-extinction ratio (η) with no assumptions on the aerosol density, which was found to be significantly different from the background boundary layer aerosol (max: $1.42\,g\,m^{-2}$ as opposed to $0.27 \pm 0.03\,g\,m^{-2}$). Using this ratio, ash mass concentration in the volcanic plume derived from LIDAR measurements was found to be $700 \pm 25\,\mu g\,m^{-3}$ when the plume was located in the FT (3000 m a.s.l. – above sea level).

This ratio could also be used to retrieve an aerosol mass concentration of $523 \pm 54\,\mu g\,m^{-3}$ on 19 April, when LIDAR observations detected the ash cloud at 3000 m a.s.l. in correspondence with model simulations (FLEXPART). On 22 April,

another ash plume entered the BL, and although it was more diluted than during the May episode, the French research aircraft ATR42 that passed over Clermont-Ferrand in the PBL confirmed the presence of particles with a supermicronic mode, again centred on a diameter of 2 µm.

5   This data set combining airborne, ground-based and remote sensing observations with dispersion model simulations shows an overall very good coherence during the volcanic eruption period, which allows a good confidence in the characteristics of the ash particles that can be derived from this unique data set.

1 Introduction

10 On 20 March 2010, a volcanic eruption started in the Fimmvörduháls pass between two central volcanoes, Eyjafjallajökull and Katla, in the southern part of Iceland, about 150 km east of Reykjavik. Lava fountains up to 200 m height characterized this first eruption phase, but the activity at Fimmvörduháls eventually ceased on 13 April 2010. A few hours later, seismic unrest was detected 20–25 km beneath the summit crater of
15 Eyjafjallajökull ($63.63°$ N, $19.62°$ W, 1666 m a.s.l.), and a long eruptive fissure opened in the above glacier ejecting a more silicic magma than before, and leading to a large phreatomagmatic eruption (Sigmundsson et al., 2010). This type of eruption is characterized by highly explosive phases due to magma-water interaction increasing pyroclasts' fragmentation, which may partly explain the very large amount of fine ash re-
20 leased into the atmosphere. The eruption has been characterized by two main phases of intense ash and gas emissions spanning 14–21 April and 1–18 May (Stohl et al., 2011), with a maximum intensity recorded on 6 May. The ash and gas emissions ceased on 24 May, after about 6 weeks of intense ash emissions. Satellite-based measurements carried out with Meteosat Second Generation (MSG) Spin-stabilised
25 Enhanced Visible and Infrared Imager (SEVIRI) and Aura-OMI sensors give a total fine ash mass estimate of 4.8 Mt centred on 4.3 µm and 0.2 Mt of sulphur dioxide (SO_2) (Gouhier et al., 2011), whereas an inversion study using SEVIRI and IASI satellite

data obtained a total fine ash mass of 8.3 Mt in the size range 2.8–28 µm (Stohl et al., 2011). Volcanic ash and gas clouds are a threat to aircraft operations (Prata and Tupper, 2009; Casadevall, 1994) and concerns about aviation safety led to repeated closure of large parts of the European airspace during periods of the Eyjafjallajökull eruption. This caused global travel chaos and the loss of billions of Euro and directly impacted millions of people.

The presence of volcanic ash in April–May 2011 has been demonstrated all over Europe through several studies. Different techniques were used aiming to determine the properties of ash particles/clouds. Airborne in-situ measurements were performed in the ash cloud by the German Falcon research aircraft (Schumann et al., 2011), measuring ash volume size distribution with a effective diameters between 0.2 and 3 µm, while the Swiss Diamond Aircraft HK36 (Bukowiecki et al., 2011) flew to track the ash plume over Switzerland and measured high particle concentrations over Zurich, up to 120 cm^{-3} for particle larger than 500 nm.

In the same study, Bukowiecki et al. present ground-based measurement at an elevated site in the Swiss Alps (Jungfraujoch). Unusual enhancements in SO$_2$ up to 25 µg m^{-3}, particulate matter (PM$_{10}$) concentrations up to 70 µg m^{-3} and a mean optical diameter around 3 ± 0.3 µm were detected. Additionally, hygroscopicity was also investigated and reveals that ash uptakes water efficiently via adsorption (Lathem et al., 2011). Another high-altitude stations recorded ash episodes combined with sulphuric dioxide and sulphuric acid enhancements in Germany (Flentje et al., 2010; Schäfer et al., 2011) while at sea-level, measurement stations also detected ashes (Lettino et al., 2011; Pitz et al., 2011).

While RADAR is intensely used close to the volcano to monitor the ash emissions, remote sensing by LIDAR is the most common technique used to detect aerosols in the atmosphere after transport far from the source. The largest ash particles settle close to the eruption site while micrometric particles can remain airborne longer and can be transported far down-wind from the volcano. Most of LIDAR measurement stations are grouped in a dedicated network (European Aerosol Research Lidar Network

to Establish an Aerosol Climatology: EARLINET) and their results are presented by Ansmann et al. (2011). They report an enhancement in the depolarization ratio, an indicator of the particle non-sphericity and in the extinction coefficient, which indicates important concentrations of large particles. Similar results are presented by several studies all over Europe (Mona et al., 2011; Emeis et al., 2011; Revuelta et al., 2011; Miffre et al., 2011; Gasteiger et al., 2011).

To convert the LIDAR signal into mass concentration, a mass-extinction ratio (η) is needed. In the studies-cited above, η values could not be calculated directly because collocated in-situ measurements were missing. For example, Miffre et al. assume an ash diameter of 10 µm and a density of 2.6 g cm^{-3} (Miffre et al., 2011). Ansmann et al. (2011) derived a particle mass concentration from a LIDAR-Photometer synergy with assumptions on density and Gasteiger et al. (2011) from a Bayesian inference statistical method with assumptions on the particle shape or on the size distribution.

In this study, we present a combination of in-situ and collocated LIDAR extinction measurements, operated by the OPGC (*Observatoire de Physique du Globe de Clermont-Ferrand*) on two different occasions during April and May 2010. The ash plume was further studied by analyzing the output from particle dispersion model simulations and airborne measurements. We present microphysical and optical properties of the volcanic ash after transport in the atmosphere and a quantitative study of the mass concentration derived from the synergy between these measurements.

2 Instrumentation and modelling

2.1 The Puy de Dôme research station

The Puy de Dôme (PdD) research station is located in the centre of France (45°46′ N, 2°57′ E) at 1465 m a.s.l. The station is equipped with state of the art instrumentation operated continuously to characterise aerosol particles and trace gases including SO$_2$ concentrations. Results showing the seasonal variation of the aerosol number size

distribution are discussed in Venzac et al. (2009).

Particle number concentrations with a diameter greater than 10 nm are measured with a butanol based CPC (model TSI 3010). Total mass concentrations of aerosol are measured with a TEOM-FDMS 8500C. The aerosol absorption coefficient σ_{abs} is measured with a Multi Angle Absorption Photometer (MAAP 5012; with a central wavelengths at 637 nm; Petzold et al., 2005), and the scattering (and backscattering) coefficient (σ_{bsca}) by a three wavelengths nephelometer (model TSI 3563 with central wavelengths of 450, 550, 700 nm) for which corrections for detection limits and truncation errors are applied (Anderson and Ogren, 1998).

The nephelometer data allow the calculation of the Ångström exponent (α) between two wavelengths:

$$\alpha = -\frac{\log \sigma_{sca\ (700\ nm)} - \log \sigma_{sca\ (450\ nm)}}{\log 700 - \log 450} \tag{1}$$

An Ångström exponent (α) value around 2 implies an aerosol size distribution with scattering (σ_{sca}) dominated by small particles (diameter $< 1\ \mu m$), while a distribution dominated by coarse particles (Dm $> 1\ \mu m$) has typically a smaller α, around 1 (Dubovik et al., 2002).

The hemispheric backscattering fraction, b, was obtained as: $b = \sigma_{bsca}/\sigma_{sca}$ and allows to calculate the asymmetry factor g with the following parameterization (Andrews et al., 2006):

$$g = -7.143889\ b^3 + 7.464439\ b^2 - 3.96356\ b + 0.9893 \tag{2}$$

Andrews et al. (2006) showed that the variable controlling the values of g is mainly the aerosol size distribution.

The MAAP and nephelometer measurements enable to calculate the single scattering albedo ϖ_0:

$$\varpi_{0\ (550\ nm)} = \frac{\sigma_{sca\ (550\ nm)}}{\sigma_{sca\ (550\ nm)} + \sigma_{abs\ (637\ nm)}} \tag{3}$$

ω_0 indicates the relative absorptivity of the aerosol, with lower values indicating stronger absorption. We assume that the absorption Ångström exponent is equal to unity (i.e. the absorption is independent from wavelength variation, i.e. $\sigma_{abs\ (637\ nm)} = \sigma_{abs\ (550\ nm)}$).

A combination of the TEOM, MAAP and nephelometer measurements can be used to calculate the mass-extinction conversion factor η at a specific wavelength λ,

$$\eta_\gamma = \frac{M}{\sigma_{sca\ (\gamma)} + \sigma_{abs\ (637\ nm)}} \tag{4}$$

where M is the total mass concentration measured by the TEOM. η is a key parameter to calculate vertically-resolved mass concentration from LIDAR measurements.

The supermicronic Particle Size Distributions (PSD) are recorded with an Optical Particle Counter (OPC, Grimm model 1.108) measuring particles in the size range $0.3 < Dm < 20\,\mu m$ over 16 channels. Submicronic PSD are detected using a Scanning Mobility Particle Sizer (SMPS; Villani et al., 2008), sizing particles in the range $10 < Dm < 500\,nm$.

SO_2 concentrations are measured by a pulsed fluorescence gas analyzer (TEI 43CTL), while nitrogen dioxide (NO_2) and nitrogen monoxide (NO) are measured by ozone chemiluminescence (TEI 42CTL), O_3 with a UV analyser (TEI 49C) and CO with a IR analyser (TEI 42 TL). The chemical composition of the aerosol is determined 2 days a week by Teflon filter samples collected following GAW (Global Atmosphere Watch) recommendation (WMO, 2003) and analysed by ionic chromatography (DIONEX). Analytical procedures are described in Bourcier et al. (2011).

2.2 LIDAR

We used a Raymetrics Rayleigh-Mie LIDAR, based on a tripled Nd:YAG frequency laser, which emits pulses of 75 mJ output energy at 355 nm with a 10 Hz repetition rate, on parallel and orthogonal polarization channels. The optical receiver is a Cassegrainian reflecting telescope with a primary mirror of 300 mm diameter and a

Full Screen / Esc

focal length of 600 mm, directly coupled, through an optical fibre, to the LIDAR signal multi-channel detection box (Papayannis et al., 2005). The vertical resolution of the raw signals is 7.5 m. The LIDAR is positioned on the roof of the OPGC, (45.76° N, 3.11° E) at 425 m a.s.l. (located 11 km east of PdD).

As the LIDAR measures both parallel and orthogonal polarization it allows us to calculate the depolarization ratio as a function of the distance r from the telescope $\delta(r)$ (Weitkamp, 2005). A large depolarization ratio indicates that the aerosol is strongly depolarizing and, thus, that particles are non-spherical. Non-spherical glass and mineral particles typical of volcanic ash generate strong laser depolarization (Sassen et al., 2007).

The LIDAR signal inversion is based on the Klett method (Klett, 1985) to obtain the aerosol extinction α_{aer} from the measured backscatter β_{aer}. The inversion needs a particle free LIDAR signal (typically between 6000 m and 8000 m) and therefore can only be realised during clear sky conditions. For each LIDAR profile, an aerosol LIDAR ratio (L_{aer}) is calculated according to the following equation:

$$L_{aer} = \frac{4 \pi}{\omega_0 \, P_{11} \, (180°)} = \frac{\alpha_{aer}}{\beta_{aer}} \tag{5}$$

with ω_0 the single scattering albedo and $P_{11} \, (180°)$ the phase function at 180° computed with a Mie code (Bond et al., 2006; Mätzler, 2002). The Mie code inputs are the size distribution and the refractive index. The size distribution is measured with the SMPS and OPC. The refractive index was obtained via an inversion of the dry scattering and absorption, using Mie theory and the measured size distribution.

2.3 Aircraft measurements

During the Eyjafjalla eruption, the French research aircraft ATR-42 was deployed over France. In order to estimate concentrations of volcanic ash in the atmosphere, two microphysical probes were mounted on the aircraft: The Passive Cavity Aerosol Spectrometer Probe (PCASP 100-X, DMT) and the Forward Scattering Spectrometer

Probe (FFSP-300, DMT) measuring in particle size ranges 0.1 µm < Dm < 3 µm and 0.3 µm < Dm < 20 µm over 30 and 31 channels, respectively. The instruments were operating outside the aircraft fuselage. From 19 to 22 April, four scientific flights were performed over France, and on 22 April, the ATR-42 flew over Clermont-Ferrand in the PBL.

2.4 FLEXPART simulations

We used the Lagrangian particle dispersion model FLEXPART (Stohl et al., 2005) to evaluate the presence of the volcanic ash cloud over our two measuring sites. FLEX-PART was run in forward mode and driven with meteorological data from the European Centre for Medium-Range Weather Forecasts (ECMWF) analyses with 0.18° × 0.18° horizontal resolution and 91 vertical model levels. The simulation accounted for gravitational particle settling as well as dry and wet deposition, but no ash aggregation processes. Formation of sulphate particles was also not simulated. The ash emission rates and heights were determined using an inversion scheme that couples a priori source information and FLEXPART model data with satellite data (Stohl et al., 2011). The ash particle size distribution included 25 particle size classes from 0.25–250 µm diameter. The model output had a spatial resolution of 0.25° × 0.25° and a vertical resolution of 250 m.

3 Results

3.1 Case 1: 18 and 19 May 2010

3.1.1 Simulated ash distribution

On 18 and 19 May, the Eyjafjalla volcanic cloud resided over Clermont-Ferrand. Figure 1 (upper panel) shows the FLEXPART simulated distribution of the ash clouds over Europe at 09:00 UTC on 18 May. The ash cloud arrived from the north and parts of

the cloud were sampled previously on 17 May over the North Sea and on 18 May over Germany by a research aircraft (Schumann et al., 2011). High ash concentrations of up to 500 µg m^{-3} were found on 17 May and still high concentrations were observed over Germany on 18 May, in relatively good agreement with the FLEXPART simulated

5 concentrations along the aircraft flight tracks (Stohl et al., 2011). Figure 1 (lower panel) shows a time-height section of the FLEXPART simulated ash mass concentrations over Clermont-Ferrand. FLEXPART is simulating volcanic ash around 3000 m a.s.l. above Clermont-Ferrand from 00:00 UTC on 18 May to 13:00 UTC on 19 May. The maximum ash mass concentration is 176 µg m^{-3} at 08:00 UTC on 19 May at 4100 m a.s.l. On

10 two occasions (on 19 May from 03:00 to 08:00 UTC and from 10:00 to 20:00 UTC), FLEXPART simulates entrainment of volcanic ash into the boundary layer.

3.1.2 LIDAR measurements

The LIDAR observations (Fig. 2a) highlight the presence of a depolarizing layer in the free troposphere (FT) at 3000 m a.s.l., from 04:00 to 10:00 UTC on 18 May, with a

15 maximum thickness of 500 m. At 10:00 UTC, cumulus clouds are formed at the same altitude as the volcanic cloud. The layer was observed again on 19 May from 06:00 (after the clouds have dissipated) to 24:00 UTC. The depolarization shows a maximum of around 19 % for 18 May and 25 % for 19 May. The LIDAR observations of the Eyjafjalla's ash cloud mostly agree in time and relative intensity with the FLEXPART

20 simulations. Nevertheless the altitude of the FLEXPART simulation is shifted by around 500 m towards higher altitudes compared to the LIDAR observations. On 19 May, the maximum intensity of both LIDAR observations and FLEXPART simulation is shown around 08:00 UTC. Moreover, the simulated cloud was dissipated when the intensity of the LIDAR observation began to decrease (around 13:00 UTC) but the presence of

25 less concentrated volcanic ash after this dissipation is not shown in FLEXPART.

The LIDAR observations also revealed twice the presence of non-spherical particles in the boundary layer. The first observation occurred between 23:30 UTC on 18 May and 04:00 UTC on 19 May, and the second between 09:45 UTC and 22:00 UTC on

19 May. While FLEXPART simulated a nearly instantaneous mixing process in the PBL at 09:00 UTC on 18 May, the non-spherical particle layer was bounded at an upper altitude of 1250 m a.s.l. at 23:30 UTC, which increases gradually with time to reach 2500 m a.s.l. at 04:00 UTC on 19 May. On the contrary, a perfect agreement was reached between simulations and observations for the cloud on 19 May with the maximum intensity of the cloud found between 15:00 and 16:00 UTC.

3.1.3 In-situ measurements at PdD

The PdD site is located about 11 km to the west of the LIDAR site, which could explain small differences in the timing and intensity of ash events at the two sites and higher topography makes the model simulation more difficult.

Figure 2b shows that SO_2 concentrations significantly increased on 18 and 19 May, reaching 2.2 ppb from 23:45 UTC on 18 May to 05:20 UTC on 19 May, and from 09:50 to 18:00 UTC on 19 May. This is above the 99th percentile calculated over the last 2 years (1.69 ppb). The enhancement of SO_2 concentration coincides exactly with the LIDAR detection of depolarizing particles detected in the PBL. NO_2, NO, CO and O_3 concentrations did not show simultaneous variations, suggesting that the SO_2 did not come from local anthropogenic sources. The NO_2/NO_x ratio is close to 1 (0.94 $\pm$ 0.06), indicating again that the pollution was not related to local traffic emissions, which are rich in NO (Soltic and Weilenmann, 2003).

Moreover, the SO_4^{2-} concentration collected on the Teflon filter from 18–19 May, 1.83 μg m^{-3}, is six times higher than the median annual concentration (0.32 μg m^{-3}) and above the 90th percentile (1.73 μg m^{-3}). The volcanic SO_2 was transported jointly with the non-spherical particles (Fig. 2b) like suggest by Thomas and Prata (2011). The presence of ash particles was confirmed by two independent devices: the TEOM instrument showed an increase of the mass concentration from 20 up to 65 μg m^{-3} (Fig. 3b) and the nephelometer light scattering measurements allowed to calculate the Ångström exponent (α), which decreased from 2 $\pm$ 0.1 to 1.1 (Fig. 3a). The asymmetry

factor g exhibits a variation similar to the Ångström exponent (not shown) with a minimum during the main volcanic event of 0.56 at 17:00 UTC on 19 May, compared to a value of 0.65 ± 0.02 outside the cloud. The single scattering albedo did not vary significantly with a value of 0.97 ± 0.01. In addition, concentrations of the total number of particles (Diameter > 10 nm) measured by the CPC 3010 increased significantly. This was related to sulphuric acid droplet nucleation events as suggested by Schumann et al. (2011) and shown by Boulon et al. (2011). Altogether, these data clearly indicate that volcanic ash was present in the boundary layer at the PdD station.

The total aerosol mass concentrations detected at PdD are also compared to the ash mass concentrations simulated by FLEXPART (Fig. 3b). Time variations of measured and simulated mass concentrations show the same pattern, although simulated ash mass concentrations are on average 4.5 times lower than the observations during the volcanic event. Two factors can explain at least partly the difference: first the background aerosol is not considered in the FLEXPART simulation. Therefore, FLEXPART is expected to show lower mass concentrations than the measurements, especially when the ash mass contributions are low. When adding the background mass concentration to the FLEXPART results as a rough estimate of the mass contributions from non-volcanic sources, the agreement is improved substantially. Secondly, FLEXPART does not simulate the formation of sulphate aerosol, which contributes to the measured aerosol mass concentration in the volcanic cloud.

The OPC and SMPS were operating from 19 May at 12:00 UTC, showing a clear increase in the 1.8 µm particle concentration measurement channel until 15:45 UTC with a maximum concentration of 2.15 cm^{-3} at 14:15 UTC (Fig. 4). It is higher than the 99th percentile (1.8 cm^{-3}) measured in 2010 and more than 10 times larger than the median (0.2 cm^{-3}). The number size distribution measured at the PdD is centred on 2 µm, corresponding to the presence of volcanic ash as detected from the LIDAR and other indicators such as the SO$_2$ concentrations. During this period, the total aerosol mass concentration derived from the size distribution (10 nm to 20 µm), assuming an ash density of 2.6 g cm^{-3} given by OPAC software for mineral (Hess et al., 1998), is

Physical and optical properties of 2010 Eyjafjallajökull volcanic eruption

M. Hervo et al.

$39.2 \pm 3.7\,\mu\mathrm{g\,m^{-3}}$. This is in good agreement, within the given uncertainties, with the TEOM mass concentration of $52 \pm 9\,\mu\mathrm{g\,m^{-3}}$ reported above. These values can be compared to the $13 \pm 4\,\mu\mathrm{g\,m^{-3}}$ of ash simulated by FLEXPART, indicating that either the volcanic aerosol would contribute by roughly 30 % of the total aerosol mass in the BL, or that the FLEXPART simulation underestimates the ash mass concentration. We may investigate the two options by considering the average aerosol mass which was measured just before the ash plume entered the BL ($21.6 \pm 4.4\,\mu\mathrm{g\,m^{-3}}$ on 18 May). By using this value as a background concentration, we achieve a 60 % contribution of the volcanic aerosol to the total mass during the plume intrusion, and a 33 % under-estimation of the FLEXPART ash simulations. A gain, the FLEXPART underestimation can be partly explained by the fact that the model does not simulate the formation of secondary aerosols.

3.1.4 Mass extinction ratio calculation

Simultaneous measurements of the in-situ aerosol total mass and of the in-situ aerosol optical properties are a unique chance to characterize the mass-to-extension ratio (η, Eq. 4) usually used for retrieving the aerosol mass from LIDAR observations. To our knowledge, in-situ measurements are the only way to calculate η with no assumption on the density of individual particles. Figure 5 shows the evolution of mass-extinction ratio η for 18 and 19 May. It clearly indicates a first enhancement from 00:00 to 04:00 UTC on 19 May, and a second increase from 10:00 to 22:00 UTC with a maximum between 15:00 and 17:00 UTC on 19 May that corresponds to the volcanic measurements previously presented.

The mean η, before the presence of the volcanic eruption cloud was $0.27\,\mathrm{g\,m^{-2}}$ (± 0.03). It is slightly higher than the values measured by Raut and Chazette around Paris ($0.21\,\mathrm{g\,m^{-2}}$) (Raut and Chazette, 2009) but similar to the median calculated all over the year at PdD ($0.28\,\mathrm{g\,m^{-2}}$).

During the onset of the event, from 10:00 to 22:00 UTC on 19 May, η increased to 0.61 g m^{-2} (±0.31) and further to a maximum of 1.42 g m^{-2} during the main event. Those values are consistent with those inverted from the multi wavelength LIDAR sounding over Maisach, Germany, during the Eyjafjalla ash observations on 17 April (1.45 g m^{-2} (0.9...2.3); Gasteiger et al., 2011). The inversion using combined photometer and LIDAR data (Ansmann et al., 2011) gave a value of 1.57 g m^{-2} for the ashes and 0.265 g m^{-2} for the fine particles. Hence, the maximum value of the mass extinction ratio measured at the PdD will be considered as representative of the volcanic particles and will be called $\eta_{volcano}$ in further calculations.

The large differences between η outside and inside the ash plume demonstrates that η is highly dependent on the aerosol properties and sensitive to varying mixtures between background aerosols and volcanic ash.

The η values that we calculated from in-situ measurements are for dry conditions (sampling relative humidity, RH, lower than 30 %). In order to apply η to the LIDAR extinction measurements, we would need to know η for humid (ambient) conditions. A simplified theoretical study of the variation of η with humidity can be performed. For an aerosol population with a mean diameter of 100 nm and a hygroscopic growth factor similar to the one of ammonium sulphate (i.e. as close as possible to the characteristics of the plume as it was detected at the Jungfraujoch; Bukowiecki et al., 2011), η only increases by 30 % when going from the dry state to a RH of 90 %. Consequently, η calculated trough the PdD dry measurements can be applied to the Lidar inversion.

If $\eta_{volcano}$ had not been appropriately estimated in the volcanic ash cloud, and instead the average value of 0.28 g m^{-2} had been used, the total particle mass retrieved would have been underestimated by roughly 80 %.

3.1.5 Mass retrievals

The retrieval of the particle mass was computed as described in Fig. 6. $\eta_{volcano}$ can be further used for particle mass retrievals in volcanic clouds when in-situ measurements are not available (typically when the ash cloud is too high for even high altitude

stations to sample it, and no airborne measurements are available). Inversions of the LIDAR signal to compute the extinction was conducted under clear sky conditions following the procedure described in Sect. 2.2. The refractive index was calculated to be $1.65 + 0.005i$ and the LIDAR ratio $52 \pm 6 \, \mathrm{sr}^{-1}$.

For the volcanic cloud at 3000 m a.s.l., during the 19 May major event in clear sky condition from 12:00 to 16:00 UTC, the mass extinction ratio for volcanic particles described in previous section was used ($\eta_{\mathrm{volcano}} = 1.42 \, \mathrm{g \, m}^{-2}$). The computed extinction was found to be $461 \pm 16 \, \mathrm{Mm}^{-1}$ at 3000 m a.s.l. which corresponds to an ash mass of $700 \pm 25 \, \mathrm{\mu g \, m}^{-3}$. This value is consistent with the mass and the extinction calculated by Ansmann and Gasteiger in Maisach, Germany, which are respectively 400–600 Mm^{-1} and ~1000 $\mathrm{\mu g \, m}^{-3}$ (Gasteiger et al., 2011; Ansmann et al., 2010).

To validate this inversion, the LIDAR value obtained at the PdD height are compared with the in-situ measurement: the extinction calculated from LIDAR measurements at 1465 m, between 12:00 and 16:00 UTC on 19 May is $862 \pm 149 \, \mathrm{Mm}^{-1}$ which correspond to a mass of $515 \pm 210 \, \mathrm{\mu g \, m}^{-3}$ with the corresponding η. It is 10 times higher than the ash mass derived from TEOM measurements for the same period of time.

The difference between in-situ and LIDAR measurements can mostly be explained by the hygroscopic effect on the particle light extinction. Indeed, the simulated extinction calculated for the dry Particle Size Distribution (PSD) measured with SMPS and GRIMM was $103 \pm 17 \, \mathrm{Mm}^{-1}$. The hygroscopic growth factor during volcanic events was found to be similar to the one of ammonium sulphate (Wise et al., 2003; Bukowiecki et al., 2011). However pure ash particles are less hygroscopic (Lathem et al., 2011). Therefore we conducted the extinction calculation after performing a virtual hygroscopic growth of the measured PSD with a growth factor of 1.7 for the submicronic mode and 1.1 for the supermicronic. We found that the extinction of the hydrated PSD was $565 \pm 141 \, \mathrm{Mm}^{-1}$. Using this procedure we are able to explain 65 % of the measured extinction instead of 17 % for dry aerosol.

Similarly, the LIDAR mass retrieval gives a much higher mass concentration than the FLEXPART simulation (Fig. 1), $700 \, \mathrm{\mu g \, m}^{-3}$ compared to $176 \, \mathrm{\mu g \, m}^{-3}$, which can

be partly explained by the difference between dry and wet mass, and partly by the likely underestimation of the volcanic aerosol mass concentration simulations (cf. Sect. 3.1.3).

3.2 Case 2: 18, 19 and 22 April 2010

3.2.1 Flexpart simulation

On 18 and 19 April, FLEXPART predicted an ash cloud over Clermont-Ferrand as shown in Fig. 7 and observed with the LIDAR (Fig. 9).

Figure 7 top panel presents the situation on 18 April simulated by FLEXPART. The ash was emitted mainly on 14–16 April, reached Central Europe on 16 April and was subsequently slowly transported to Western Europe and resided mainly over France on 18 and 19 April (Stohl et al., 2011). The bottom panel presents the time series of the simulated ash mass over Clermont-Ferrand as function of altitude and time. Two layers at 3500 m and 4700 m a.s.l. are predicted. The 3500 m layer was simulated from 18 April at 15:00 UTC to 19 April at 09:00 UTC with mass concentrations around 50 μg m^{-3} This layer progressively became thicker with time, from a few hundred metres until a width of around 1 km. The 4700 m layer was observed with a stronger intensity from 20:00 UTC on 18 April to 06:00 UTC on 19 April. At a maximum concentration of 247 μg m^{-3}, it was simulated with a thickness of 1 km. The simulation shows a layer of lower concentration in the planetary boundary layer with a maximum concentration of 40 μg m^{-3}.

Figure 8 represents the dispersion of ashes simulated by FLEXPART for 22 April. Ash was simulated only in the PBL. The concentrations predicted are significantly lower than on 18 April with a maximum concentration of 18 μg m^{-3} at 06:00 UTC.

3.2.2 LIDAR observations

Figure 9 shows the depolarization ratio time series for 18–19 April where two highly depolarizing aerosol layers, indicating non-spherical particles, are detected at 4700 m and 3000 m a.s.l. The most depolarizing layer at 4700 m appears at 16:00 UTC, and was progressively dissipated in the morning of 19 April and had a maximum depolarization ratio of 17 %, while the layer at 3000 m reached a maximum depolarization ratio of 16 % between 05:00 a.m. and noon of 19 April. A low depolarizing layer observed at 1100 m is also visible.

The FLEXPART simulation (Fig. 7) shows high similarities with the LIDAR measurements, but also some discrepancies. The layer detected at 3000 m was simulated by FLEXPART with the same thickness and time of occurrence. The appearance of the 4700 m layer is however observed about 5 h earlier with the LIDAR than simulated by FLEXPART. Still, the altitude of the layer is well simulated. The layer detected at 1000 m a.s.l. by the LIDAR has also been simulated at the same time but with a greater thickness. The simulation shows that the ash particles were mixed in the planetary boundary layer by the model but the LIDAR observations show a strong stratification during the night and the presence of the depolarizing particles at a well delimited altitude. In-situ measurements at the PdD station did not show any strong signal that could indicate that the cloud entered the PBL, in agreement with the LIDAR observations, and contrarily to the FLEXPART simulation. Some of the discrepancy between observations and simulation can be explained partly by the complex transport of the ash cloud. The ash was emitted 3–5 days earlier and transported slowly to Western Europe where it resided over France for a few days. This complicated and long-range transport of the emissions makes it difficult for the model to accurately simulate the ash distribution and can explain the 5 h time delay as well as the ash layer in the PBL not in accordance with the observations. In comparison, for the May event previously shown, the ash transport was quicker and more directly towards the observation sites.

This demonstrates the uncertainties in the model simulations, which increase with time during the ash transport from its source.

The LIDAR depolarization ratio on 22 April in the early morning highlights the presence of altocumulus clouds between 4000 m and 7500 m (Fig. 10). After dissipation of the clouds at 06:30 UTC, a depolarizing signature was still present, at 5500 m and 4000 m, probably ash from the Eyjafjalla eruption. However FLEXPART doesn't show any ash at this altitude hence, they might be other non-spherical particles such as dust particles transported during this period from Asian deserts (Uno et al., 2011).

At the top of the nocturnal boundary layer at 1000 m, another ash layer was present from midnight to 04:00 UTC. At 09:00 UTC, non-spherical particles rose in the convective boundary layer and progressively reached 3000 m. These non-spherical particles show a depolarization ratio which is lower (7 %) than the one measured directly in the ash cloud on 18 and 19 April (16 %). However, their presence corroborate the FLEXPART results showing ash traces in the PBL, and a low depolarization ratio might just indicate that ash particles are highly diluted and mixed with other background aerosol particles in the BL .

3.2.3 Aircraft and ground-based measurements

Four scientific flights were performed over France between 19 and 22 April mainly over Paris and Toulouse. On 22 April, the ATR-42 flew between Rouen and Toulouse. Only during this flight, the ATR-42 passed over Clermont-Ferrand between 700 m and 1700 m, measuring in-situ particle size distributions. The aircraft trajectory is presented in Fig. 11, with boundary layer measurement periods highlighted in red.

The FSSP 300 number size distribution measurements obtained along the flight track on 22 April are presented in Fig. 12a as a function of time. High particle concentrations both in the submicronic ($\sim$100 nm) and in the supermicronic ($\sim$2 µm) modes are detected in the planetary boundary layer (PBL). While this is expected for the submicronic particles, coarse particles around 2 µm are not usually found in the PBL to that extent (1 cm^{-3}). This unusual mode was also measured during the previous flights

performed over France and is suspected to be volcanic ash externally mixed in the PBL with pollution or sulphate particles formed from volcanic SO_2, as also shown by the FLEXPART simulation at that time (Fig. 8).

Figure 12b shows the mean aerosol number size distributions measured in the PBL over Clermont-Ferrand by PCASP (blue curve) and FSSP 300 (green curve) probes and by the OPC at the PdD station (red curve). FSSP and OPC measurements highlight the coarse mode mentioned above. Unlike on 18 and 19 April, a coarse mode aerosol was detected by OPC measurements at the PdD during the period from 20–22 April, when the volcanic ash had descended into the PBL.

The volume size distribution measurements at the OPC 2.5 µm channel (Fig. 13) give a concentration of $0.8\,cm^{-3}$ at 11:30 UTC on 22 April, when the airplane was over Clermont-Ferrand. This concentration exceeds the 90th percentile measured at the station in the year 2010 ($0.68\,cm^{-3}$) and is substantially higher than the annual median ($0.19\,cm^{-3}$). This 2 µm mode was observed from 20 April to 22 April, with still concentrations substantially higher than the annual median but lower than concentrations observed during the main volcanic events on 19 May (Fig. 4).

However the effective diameter is $280\pm20\,nm$ from 18 to 22 April. It suggests that the volume size distribution is not dominated by the ashes but by the accumulation mode centred on 350 nm. Correspondingly, as already mentioned, the LIDAR measured rather low depolarization ratio (7 %) on 22 April, compared to the ratio detected in the ash clouds on 18 and 19 April (16 %). This indicates that the ash concentrations were substantially lower on 22 April than on 18 and 19 April. It appears that volcanic ash transported to Europe at rather high altitudes subsided and eventually reached the PBL where it mixed with particles already present. During the four flights performed over France from 19 to 22 April, this coarse mode was always measured in the PBL but never in the FT.

The effective diameter calculated from FFSP airborne measurements is 0.6 µm. This is consistent with the airborne measurements in the Eyjafjalla cloud by the German DLR aircraft, which observed an effective diameter between 0.2 and 3 µm (Schumann

et al., 2011). This can be explained by the preferential removal of larger particles by gravitational settling. The ash cloud sampled on 22 April was particularly aged and mixed with ambient aerosol, thus, a small effective diameter is expected. Airborne PSD measurements lead to a mass of $21 \, \mu g \, m^{-3}$ with the OPAC density for transported mineral of $2.6 \, g \, cm^{-3}$ (Hess et al., 1998). This might be an underestimation as the smallest measured particle size was $0.1 \, \mu m$.

The simultaneous in-situ measurements at PdD, give a particle size distribution centred at $2.5 \, \mu m$ with a mass concentration measured by the TEOM of $40 \, \mu g \, m^{-3}$ on 22 April at 11:30 UTC. Flentje et al. (2010) observed similar enhancement in Germany. The mass concentration did not show an important variation on 22 April, when the volcanic plume was observed, and thus does not allow us to calculate the fraction of volcanic ashes. The mean Ångström exponent (α) on 22 April was 1.99 ± 0.09. Thus the scattering was not dominated by the ash but by smaller particles. Consequently the calculated mass extinction ratio η was low compared to $\eta_{volcano}$: $0.21 \pm 0.06 \, g \, m^{-2}$ instead of $1.42 \, g \, m^{-2}$.

3.2.4 Mass retrieval

The mass retrieval in the volcanic cloud on 19 April, from LIDAR measurements (as described in Sect. 3.1.5) lead to a mean extinction of $369 \pm 38 \, Mm^{-1}$ and a mass of $523 \pm 54 \, \mu g \, m^{-3}$ at 3000 m a.s.l. from 03:30 to 05:00 UTC.

Miffre et al., through a slightly different LIDAR inversion retrieved an extinction of $187 \pm 34 \, Mm^{-1}$ and a mass concentration of $270 \pm 70 \, \mu g \, m^{-3}$ on 17 April over Lyon, 140 km east from Clermont-Ferrand (Miffre et al., 2011). On 19 April the mass concentration inverted was around $100 \, \mu g \, m^{-3}$ at 5000 m. They used the assumptions of a fixed LIDAR ratio of $55 \, sr^{-1}$, a density of $2600 \, kg \, m^{-3}$ and a diameter of 10 μm dominating the mass concentration. These assumptions and the different configuration of the volcanic cloud at that time, can explain the difference of mass retrieval.

On 22 April at 12:00 UTC, the extinction was $275 \pm 56 \, Mm^{-1}$ at the height of PdD. The volcanic mass-extinction ratio $\eta_{volcano}$ cannot be applied in this case since ash was very

Physical and optical properties of 2010 Eyjafjallajökull volcanic eruption

M. Hervo et al.

Title Page

Abstract | Introduction

Conclusions | References

Tables | Figures

◄ | ►|

◄ | ►

Back | Close

Full Screen / Esc

Printer-friendly Version

Interactive Discussion

diluted in the PBL. Moreover, both the low depolarization ratio, effective diameter and the high Ångström exponent confirm the hypothesis that non-volcanic particles were dominant. Thus we used the mass-extinction calculated at the same time. The mass retrieved is $54 \pm 9\,\mu\mathrm{g\,m^{-3}}$. It is slightly higher than the in-situ measurements and can be explained by the hygroscopic growth of the particles.

FLEXPART concentrations are still lower than the mass derived from LIDAR measurements and can be explained by both the presence of non-volcanic aerosols and by the fact that FLEXPART does not simulate hygroscopic growth of the particles and formation of secondary aerosols. Moreover the observations of the ash cloud over Germany from the 17 to 22 April highlight the fact that volcanic particles contributed, on average, only 30.2 % of the total mass concentration (Pitz et al., 2011).

4   Conclusions

This paper presents in-situ and ground-based remote-sensing measurements of the Eyjafjallajökull volcanic aerosol cloud in the free troposphere (FT) and Planetary Boundary Layer (PBL) over Clermont-Ferrand.

The highly depolarizing signature (indicating non-spherical particles) of volcanic ash was detected by LIDAR on 18 and 19 May at 3000 m, and on 18, 19 and 22 April 2010, between 3000 and 4700 m. The presence of ash simulated by FLEXPART agreed well with the observations, with small differences between simulated and observed altitudes of the ash cloud (shifted upward by 500 m in the model during the May event) or in the timing of the cloud arrival (shifted by 5 h in the model).

On both the May and April events, the ash cloud ended to enter the PBL, as shown both by the LIDAR measurements and the FLEXPART simulation. Consequently, the ash could be observed with a suite of in-situ measurement instruments at the Puy de Dôme (PdD 1465 m) station, which allowed us to characterise the microphysical and optical properties of the particles. In the ash clouds high SO_2 concentrations were observed, which were not correlated with NO_2 concentrations, thus confirming

the volcanic origin of the air mass. The ground-based measurements showed that ash particles had a supermicronic mode around 2 µm, also detected at this size by airborne measurement during the April event.

During the May event, the concentration of particles with a diameter larger than 10 nm detected at the Puy de Dôme was up to 24 000 cm^{-3}, and the mass concentration reached 65 µg m^{-3}. Volcanic particles are estimated to contribute around 60 % of this mass during May. During the April event, the volcanic plume was too diluted to calculate the ash contribution. Comparison with the volcanic particle mass simulated with FLEXPART shows that the model underestimates the volcanic aerosol contribution by 33 % in May. It can be partly explained by the formation of secondary particles not taken into account in the model.

Because the May event appeared to be much more impacted by ash particles when they entered the PBL, we used this data set to characterize the optical parameters of the ash. Dry extinction was up to 200 Mm^{-1}. The minima of the Ångström coefficient at 1.1 and the asymmetry factor of 0.56 are indicative of coarse mode particles. The constant single scattering albedo of 0.97 does not suggest the ash to be strongly absorbing. Moreover, when the ash concentration appears the most concentrated, we calculate for the first time an in-situ volcanic mass to extinction ratio η.

This ratio was then used for mass concentration inversion of volcanic ash with LIDAR measurements. We found a mass concentration of 700 ± 25 µg m^{-3} in May and 523 ± 54 µg m^{-3} in April, which is clearly higher than the in-situ mass concentrations. The discrepancy could be explained for 65 % by the hygroscopic growth of the particles as seen by the LIDAR, while the mass detected in-situ is a dry mass.

Mass concentrations retrieved from the LIDAR are also higher than the FLEXPART simulation and can be partly explained, again, by the hygroscopic growth of the particles and the formation of secondary aerosols, not taken into account in the simulation, and partly by the slight underestimation of the volcanic aerosol particle mass from the model simulations.

This work has shown that the time scale and localisation of simulated ash clouds agree relatively well with both remote sensing and in-situ observations (ground-based and airborne), although simulations might be slightly underestimating the ash concentrations by 33 %. The coinciding remote sensing and ground-based measurements will allow for a better ash particle mass retrieval from LIDAR soundings in the future, although some discrepancies still exist between in-situ and remote sensing retrievals. At last, this study highlights the importance of taking into account the impact of given aerosol types hygroscopicity on light scattering, and also the need of a climatology of mass extinction ratio to retrieve the aerosol mass from LIDAR measurements.

CNRS INSU

Institut national des **sciences** de **l'Univers**

References

Anderson, T. and Ogren, J.: Determining Aerosol Radiative Properties Using the TSI 3563 Integrating Nephelometer, Aerosol Sci. Tech., 29, 57–69, 1998.

Andrews, E., Sheridan, P. J., Fiebig, M., McComiskey, A., Ogren, J. A., Arnott, P., Covert, D., Elleman, R., Gasparini, R., Collins, D., Jonsson, H., Schmid, B., and Wang, J.: Comparison of methods for deriving aerosol asymmetry parameter, J. Geophys. Res., 111, D05S04, doi:10.1029/2004jd005734, 2006.

Ansmann, A., Tesche, M., Groß, S., Freudenthaler, V., Seifert, P., Hiebsch, A., Schmidt, J., Wandinger, U., Mattis, I., Müller, D., and Wiegner, M.: The 16 April 2010 major volcanic ash plume over central Europe: EARLINET lidar and AERONET photometer observations at Leipzig and Munich, Germany, Geophys. Res. Lett., 37, L13810, doi:10.1029/2010gl043809, 2010.

Ansmann, A., Tesche, M., Seifert, P., Groß, S., Freudenthaler, V., Apituley, A., Wilson, K. M., Serikov, I., Linné, H., Heinold, B., Hiebsch, A., Schnell, F., Schmidt, J., Mattis, I., Wandinger, U., and Wiegner, M.: Ash and fine-mode particle mass profiles from EARLINET-AERONET observations over central Europe after the eruptions of the Eyjafjallajökull volcano in 2010, J. Geophys. Res., 116, D00U02, doi:10.1029/2010jd015567, 2011.

Bond, T. C., Habib, G., and Bergstrom, R. W.: Limitations in the enhancement of visible light absorption due to mixing state, J. Geophys. Res.-Atmos., 111, D20211, doi:10.1029/2006jd007315, 2006.

Boulon, J., Sellegri, K., Hervo, M., and Laj, P.: Observations of nucleation of new particles in a volcanic plume, P. Natl. Acad. Sci., doi:10.1073/pnas.1104923108, 2011.

Bukowiecki, N., Zieger, P., Weingartner, E., Jurán-yi, Z., Gysel, M., Neininger, B., Schneider, B., Hueglin, C., Ulrich, A., Wichser, A., Henne, S., Brunner, D., Kaegi, R., Schwikowski, M., Tobler, L., Wienhold, F. G., Engel, I., Buchmann, B., Peter, T., and Baltensperger, U.: Ground-based and airborne in-situ measurements of the Eyjafjallajökull volcanic aerosol plume in Switzerland in spring 2010, Atmos. Chem. Phys. Discuss., 11, 12949–13002, doi:10.5194/acpd-11-12949-2011, 2011.

Casadevall, T. J.: The 1989–1990 eruption of redoubt volcano, Alaska – Impacts on aircraft operations, J. Volcanol. Geotherm. Res., 62, 301–316, 1994.

Dubovik, O., Holben, B., Eck, T. F., Smirnov, A., Kaufman, Y. J., King, M. D., Tanre, D., and Slutsker, I.: Variability of absorption and optical properties of key aerosol types observed in worldwide locations, J. Atmos. Sci., 59, 590–608, 2002.

Emeis, S., Forkel, R., Junkermann, W., Schäfer, K., Flentje, H., Gilge, S., Fricke, W., Wiegner, M., Freudenthaler, V., Groß, S., Ries, L., Meinhardt, F., Birmili, W., Münkel, C., Obleitner, F., and Suppan, P.: Measurement and simulation of the 16/17 April 2010 Eyjafjallajökull volcanic ash layer dispersion in the northern Alpine region, Atmos. Chem. Phys., 11, 2689–2701, doi:10.5194/acp-11-2689-2011, 2011.

Physical and optical properties of 2010 Eyjafjallajökull volcanic eruption

M. Hervo et al.

Title Page

Abstract	Introduction
Conclusions	References
Tables	Figures

Back | Close

Full Screen / Esc

Printer-friendly Version

Interactive Discussion

Flentje, H., Claude, H., Elste, T., Gilge, S., Köhler, U., Plass-Dülmer, C., Steinbrecht, W., Thomas, W., Werner, A., and Fricke, W.: The Eyjafjallajökull eruption in April 2010 - detection of volcanic plume using in-situ measurements, ozone sondes and lidar-ceilometer profiles, Atmos. Chem. Phys., 10, 10085–10092, doi:10.5194/acp-10-10085-2010, 2010.

Gasteiger, J., Groß, S., Freudenthaler, V., and Wiegner, M.: Volcanic ash from Iceland over Munich: mass concentration retrieved from ground-based remote sensing measurements, Atmos. Chem. Phys., 11, 2209–2223, doi:10.5194/acp-11-2209-2011, 2011.

Gouhier, M. P. L. Harris, P., Guéhenneux, Y., Bergès, J. C., and Cacault, P.: Properties of the Eyjafjallajökull ash cloud: insights from satellite-based measurements, Geology, in review, 2011.

Hess, M., Koepke, P., and Schult, I.: Optical properties of aerosols and clouds: The software package OPAC, B. Am. Meteorol. Soc., 79, 831–844, 1998.

Klett, J. D.: Lidar inversion of variable backscatter extinction ratios, Appl. Optics, 24, 1638–1643, 1985.

Lathem, T. L., Kumar, P., Nenes, A., Dufek, J., Sokolik, I. N., Trail, M., and Russell, A.: Hygroscopic properties of volcanic ash, Geophys. Res. Lett., 38, L11802, doi:10.1029/2011gl047298, 2011.

Lettino, A., Caggiano, R., Fiore, S., Macchiato, M., Sabia, S., and Trippetta, S.: Eyjafjallajökull volcanic ash in southern Italy, Atmos. Environ., in press, 2011.

Mätzler, C.: MATLAB functions for Mie scattering and absorption, Research Report 2002–2008 Institut für Angewandte Physik, Bern, 2002.

Miffre, A., David, G., Thomas, B., Rairoux, P., Fjaeraa, A. M., Kristiansen, N. I., and Stohl, A.: Volcanic aerosol optical properties and phase partitioning behavior after long-range advection characterized by UV-Lidar measurements, Atmos. Environ., in press, 2011.

Mona, L., Amodeo, A., D'Amico, G., Giunta, A., Madonna, F., and Pappalardo, G.: Multiwavelength Raman lidar observations of the Eyjafjallajökull volcanic cloud over Potenza, Southern Italy, Atmos. Chem. Phys. Discuss., 11, 12763–12803, doi:10.5194/acpd-11-12763-2011, 2011.

Papayannis, A., Balis, D., Amiridis, V., Chourdakis, G., Tsaknakis, G., Zerefos, C., Castanho, A. D. A., Nickovic, S., Kazadzis, S., and Grabowski, J.: Measurements of Saharan dust aerosols over the Eastern Mediterranean using elastic backscatter-Raman lidar, spectrophotometric and satellite observations in the frame of the EARLINET project, Atmos. Chem. Phys., 5, 2065–2079, doi:10.5194/acp-5-2065-2005, 2005.

Title Page

Abstract | Introduction

Conclusions | References

Tables | Figures

◄ | ►

◄ | ►

Back | Close

Full Screen / Esc

Printer-friendly Version

Interactive Discussion

Petzold, A., Schloesser, H., Sheridan, P. J., Arnott, W. P., Ogren, J. A., and Virkkula, A.: Evaluation of Multiangle Absorption Photometry for Measuring Aerosol Light Absorption, Aerosol Sci. Tech., 39, 40–51, 2005.

Pitz, M., Gu, J., Soentgen, J., Peters, A., and Cyrys, J.: Particle size distribution factor as an indicator for the impact of the Eyjafjallajökull ash plume at ground level in Augsburg, Germany, Atmos. Chem. Phys. Discuss., 11, 16417–16437, doi:10.5194/acpd-11-16417-2011, 2011.

Prata, A. and Tupper, A.: Aviation hazards from volcanoes: the state of the science, Nat. Hazards, 51, 239–244, doi:10.1007/s11069-009-9415-y, 2009.

Raut, J.-C. and Chazette, P.: Assessment of vertically-resolved PM_{10} from mobile lidar observations, Atmos. Chem. Phys., 9, 8617–8638, doi:10.5194/acp-9-8617-2009, 2009

Revuelta, M. A., Sastre, M., Fernández, A. J., Martin, L., García, R., Gomez-Moreno, F. J., Artiñano, B., Pujadas, M., and Molero, F.: Characterization of the Eyjafjallajökull volcanic plume over the Iberian Peninsula by lidar remote sensing and ground level data collection, Atmos. Environ., accepted, 2011.

Sassen, K., Zhu, J., Webley, P., Dean, K., and Cobb, P.: Volcanic ash plume identification using polarization lidar: Augustine eruption, Alaska, Geophys. Res. Lett., 34, L08803, doi:10.1029/2006gl027237, 2007.

Schäfer, K., Thomas, W., Peters, A., Ries, L., Obleitner, F., Schnelle-Kreis, J., Birmili, W., Diemer, J., Fricke, W., Junkermann, W., Pitz, M., Emeis, S., Forkel, R., Suppan, P., Flentje, H., Wichmann, H. E., Gilge, S., Meinhardt, F., Zimmermann, R., Weinhold, K., Soentgen, J., Münkel, C., Freuer, C., and Cyrys, J.: Influences of the 2010 Eyjafjallajökull volcanic plume on air quality in the northern Alpine region, Atmos. Chem. Phys. Discuss., 11, 9083–9132, doi:10.5194/acpd-11-9083-2011, 2011.

Schumann, U., Weinzierl, B., Reitebuch, O., Schlager, H., Minikin, A., Forster, C., Baumann, R., Sailer, T., Graf, K., Mannstein, H., Voigt, C., Rahm, S., Simmet, R., Scheibe, M., Lichtenstern, M., Stock, P., Rüba, H., Schäuble, D., Tafferner, A., Rautenhaus, M., Gerz, T., Ziereis, H., Krautstrunk, M., Mallaun, C., Gayet, J.-F., Lieke, K., Kandler, K., Ebert, M., Weinbruch, S., Stohl, A., Gasteiger, J., Groß, S., Freudenthaler, V., Wiegner, M., Ansmann, A., Tesche, M., Olafsson, H., and Sturm, K.: Airborne observations of the Eyjafjalla volcano ash cloud over Europe during air space closure in April and May 2010, Atmos. Chem. Phys., 11, 2245–2279, doi:10.5194/acp-11-2245-2011, 2011.

Sigmundsson, F., Hreinsdottir, S., Hooper, A., Arnadottir, T., Pedersen, R., Roberts, M. J.,

Title Page

Abstract | Introduction

Conclusions | References

Tables | Figures

◄ | ►

Back | Close

Full Screen / Esc

Printer-friendly Version

Interactive Discussion

Oskarsson, N., Auriac, A., Decriem, J., Einarsson, P., Geirsson, H., Hensch, M., Ofeigsson, B. G., Sturkell, E., Sveinbjornsson, H., and Feigl, K. L.: Intrusion triggering of the 2010 Eyjafjallajokull explosive eruption, Nature, 468, 426–253, doi:10.1038/nature09558, 2010.

Soltic, P. and Weilenmann, M.: NO_2/NO emissions of gasoline passenger cars and light-duty trucks with Euro-2 emission standard, Atmos. Environ., 37, 5207–5216, doi:10.1016/j.atmosenv.2003.05.003, 2003.

Stohl, A., Forster, C., Frank, A., Seibert, P., and Wotawa, G.: Technical note: The Lagrangian particle dispersion model FLEXPART version 6.2, Atmos. Chem. Phys., 5, 2461–2474, doi:10.5194/acp-5-2461-2005, 2005.

Stohl, A., Prata, A. J., Eckhardt, S., Clarisse, L., Durant, A., Henne, S., Kristiansen, N. I., Minikin, A., Schumann, U., Seibert, P., Stebel, K., Thomas, H. E., Thorsteinsson, T., Tørseth, K., and Weinzierl, B.: Determination of time- and height-resolved volcanic ash emissions and their use for quantitative ash dispersion modeling: the 2010 Eyjafjallajökull eruption, Atmos. Chem. Phys., 11, 4333–4351, doi:10.5194/acp-11-4333-2011, 2011.

Thomas, H. E. and Prata, A. J.: Sulphur dioxide as a volcanic ash proxy during the April-May 2010 eruption of Eyjafjallajökull Volcano, Iceland, Atmos. Chem. Phys., 11, 6871–6880, doi:10.5194/acp-11-6871-2011, 2011.

Uno, I., Eguchi, K., Yumimoto, K., Liu, Z., Hara, Y., Sugimoto, N., Shimizu, A., and Takemura, T.: Large Asian dust layers continuously reached North America in April 2010, Atmos. Chem. Phys., 11, 7333–7341, doi:10.5194/acp-11-7333-2011, 2011.

Venzac, H., Sellegri, K., Villani, P., Picard, D., and Laj, P.: Seasonal variation of aerosol size distributions in the free troposphere and residual layer at the puy de Dôme station, France, Atmos. Chem. Phys., 9, 1465–1478, doi:10.5194/acp-9-1465-2009, 2009.

Villani, P., Picard, D., Michaud, V., Laj, P., and Wiedensohler, A.: Design and validation of a volatility hygroscopic tandem differential mobility analyzer (VH-TDMA) to characterize the relationships between the thermal and hygroscopic properties of atmospheric aerosol particles, Aerosol Sci. Tech., 42, 729–741, doi:10.1080/02786820802255668, 2008.

Weitkamp, C.: Lidar: range-resolved optical remote sensing of the atmosphere, Springer Science + Business Media, 2005.

WMO: WMO/GAW Aerosol Measurement procedures guidelines and recommendations, WMO TD, No. 1178, 2003.
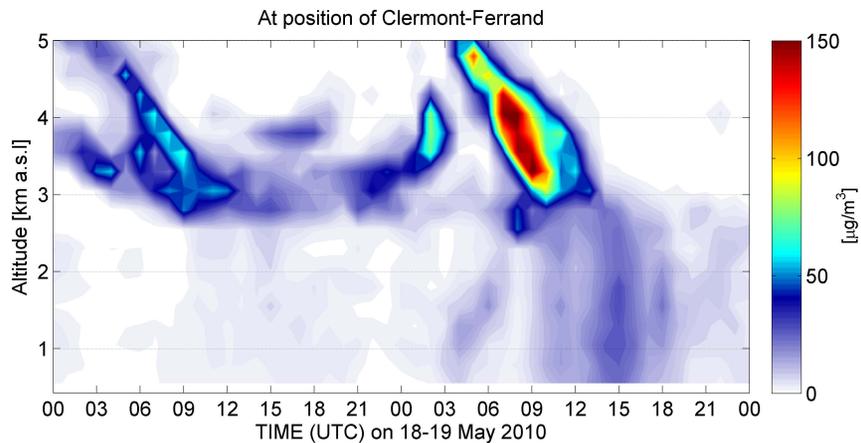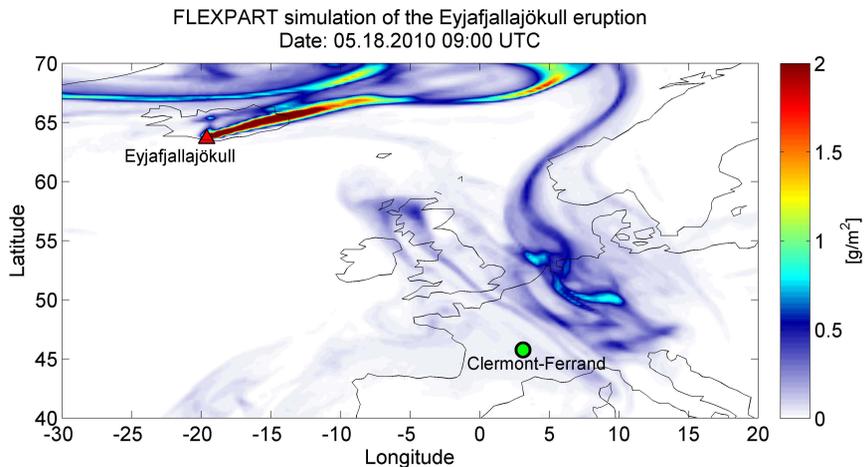
Fig. 1. FLEXPART simulated ash cloud. Total ash column load on 18 April 23:00 UTC (upper panel), and simulated vertical distribution of ash over Clermont-Ferrand for 18–19 April (lower panel).
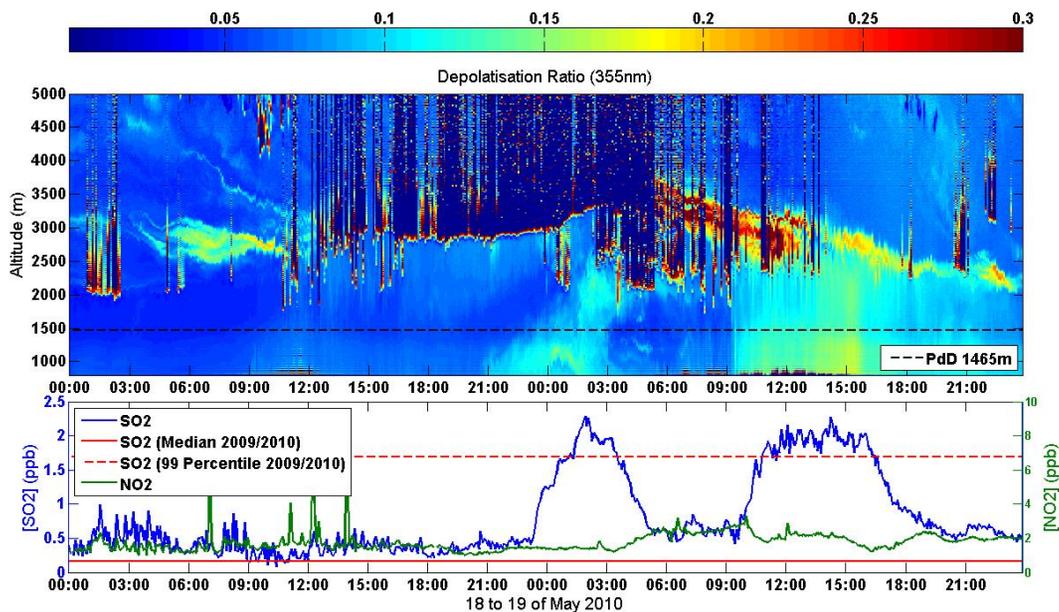
Fig. 2. Top panel: time series of depolarization ratio derived from the LIDAR data. The black dashed line represents the height of the PdD measurement station (1465 m a.s.l.). Bottom panel: SO_2 and NO_2 concentrations at PdD for the same period. The red dash line indicates the 99-percentile of SO_2 concentrations observed in 2009 and 2010 and the continuous red line the median.
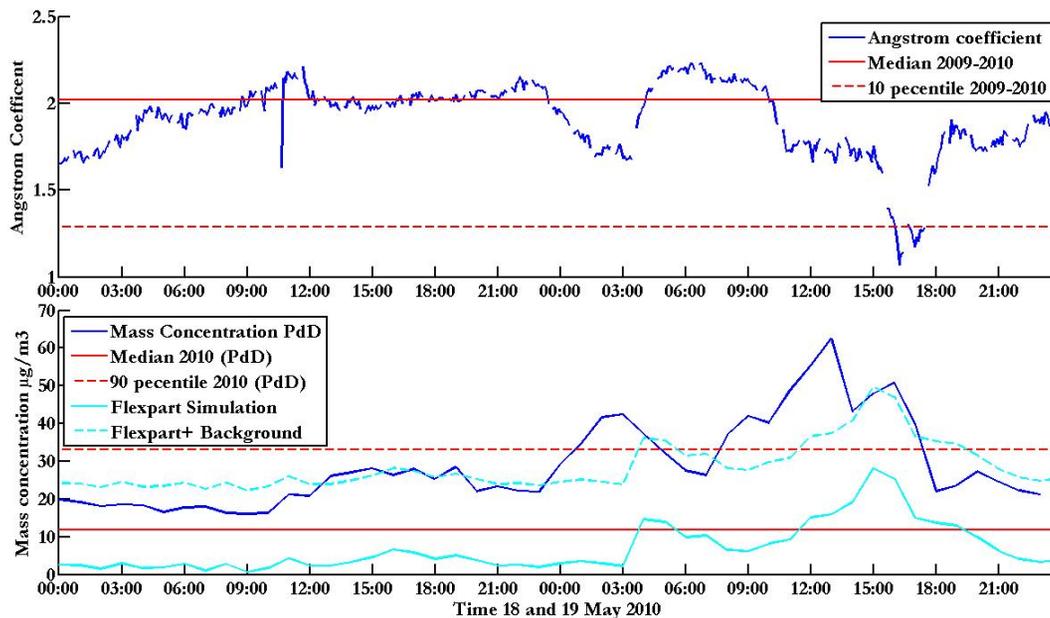
Fig. 3. Top panel: Ångstrom coefficient for the 18 and 19 May. The continuous red line indicates the median observed in 2009 and 2010 and the dotted line represents the 10th percentile. Bottom panel: Mass concentration in $\mu g \, m^{-3}$ measured by the TEOM in blue and simulated by FLEXPART at the PdD height for the same date. The continuous red line indicates the median measured in 2010 and the dotted line represents the 90th percentile. The dotted cyan line represents the FLEXPART simulated mass plus 1 the background measured before the volcanic event.
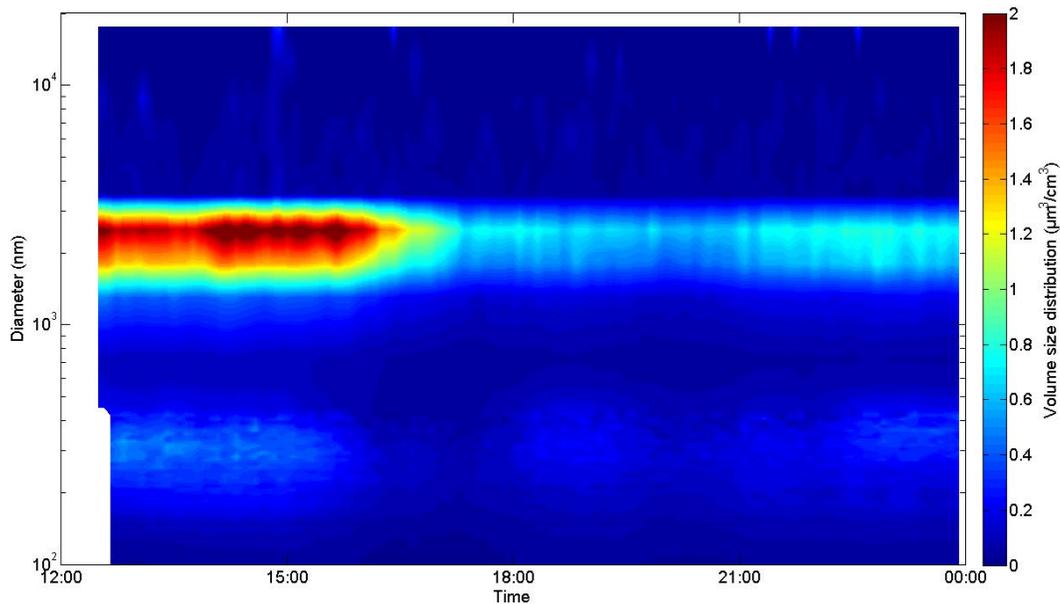
Fig. 4. Particle volume size distribution measured by a SMPS and Grimm OPC on 19 May 2010 at the 5 Puy de Dôme.
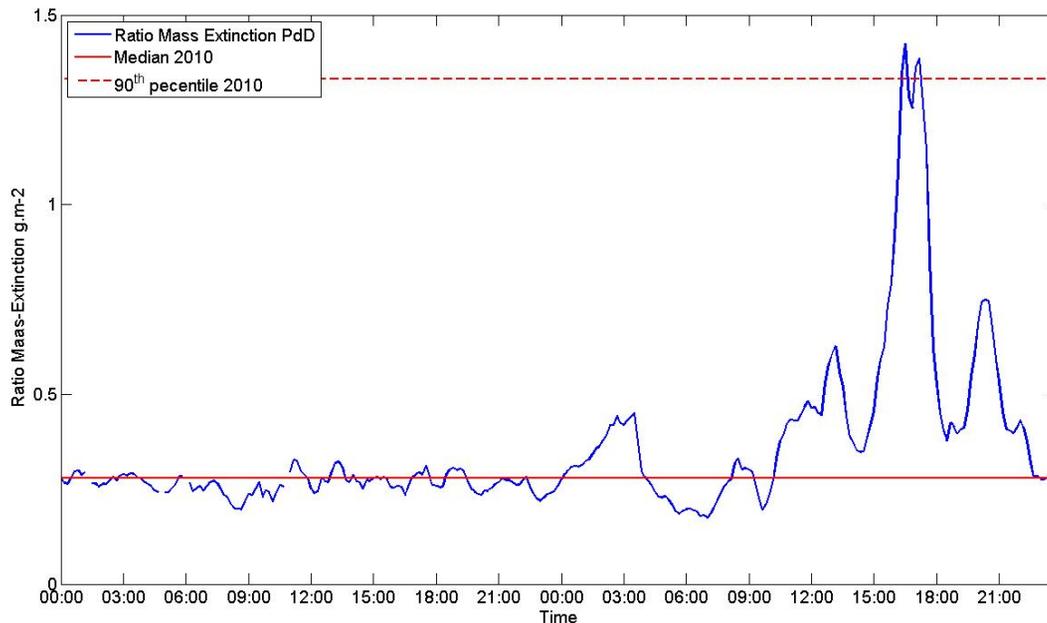
Fig. 5. Mass extinction ratio η calculated at 355 nm for the 18 to 19 May 2010. The continuous red line represents the median and the dashed red line the 90th percentile calculated using all data for the year 2010.
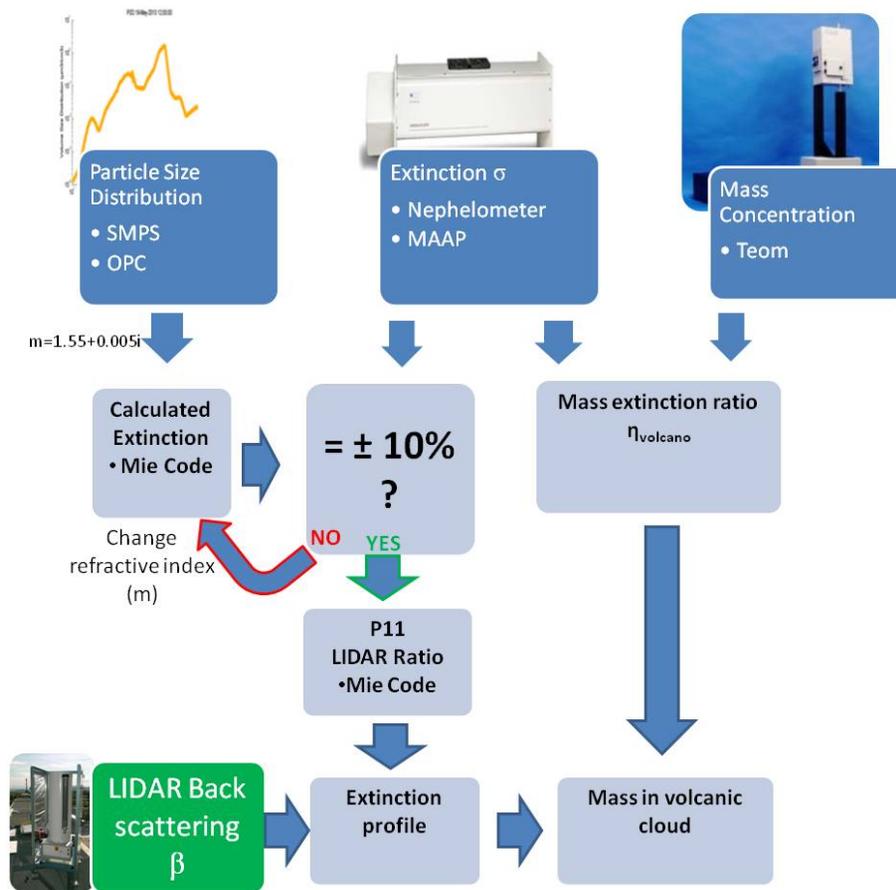
Fig. 6. Diagram of the volcanic mass retrieval. Dark-blue squares correspond to PdD in-situ measurements during the volcanic event, green to ground-based measurements, and light blue to calculated products.

Fig. 7. FLEXPART simulated ash cloud. Total ash column load on 18 April 23:00 UTC (upper panel), and simulated vertical distribution of ash over Clermont-Ferrand for 18–19 April (lower panel).
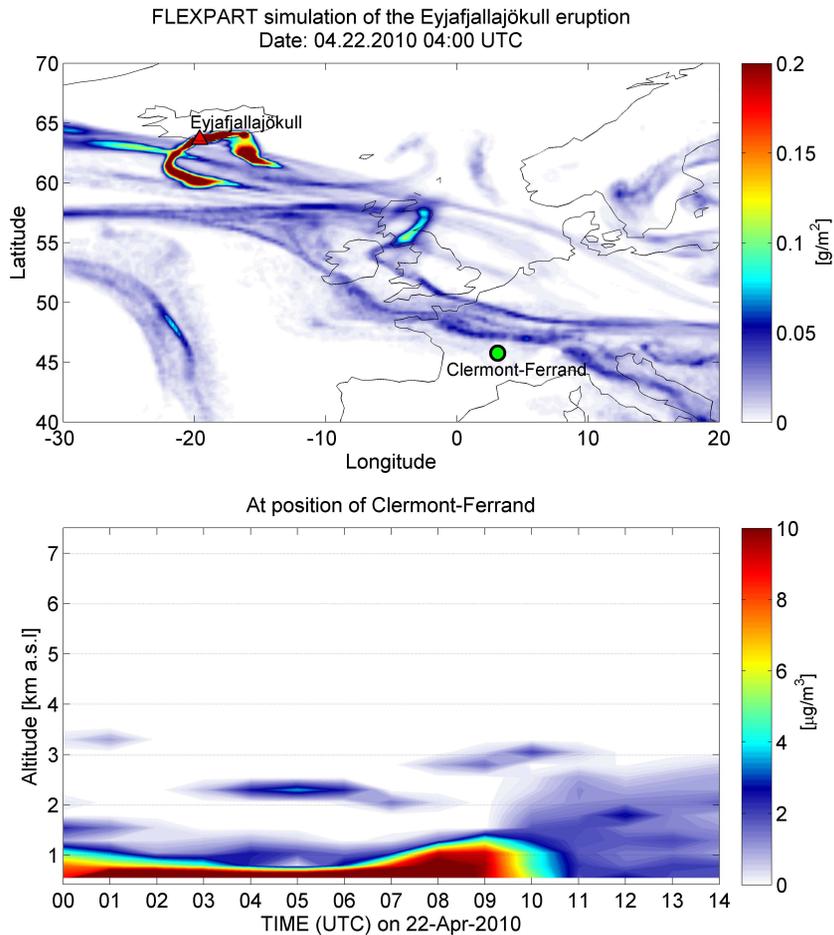
Fig. 8. FLEXPART simulated ash cloud. Total ash column load on 22 April 04:00 UTC (upper panel), and simulated vertical distribution of ash over Clermont-Ferrand for 22 April (lower panel).

Title Page

Abstract | Introduction

Conclusions | References

Tables | Figures

|◀ | ▶|

◀ | ▶

Back | Close

Full Screen / Esc

Printer-friendly Version

Interactive Discussion
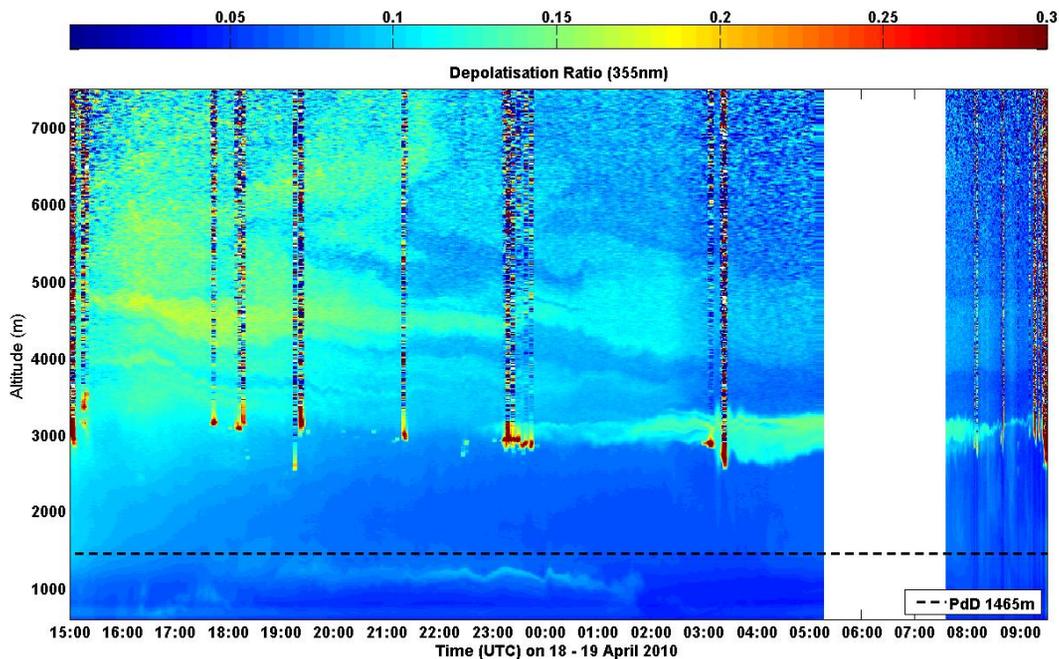
Fig. 9. Time series of the colour-coded depolarization ratio as a function of altitude for 18 to 19 April 2010. The black dotted line corresponds to the altitude of PdD.
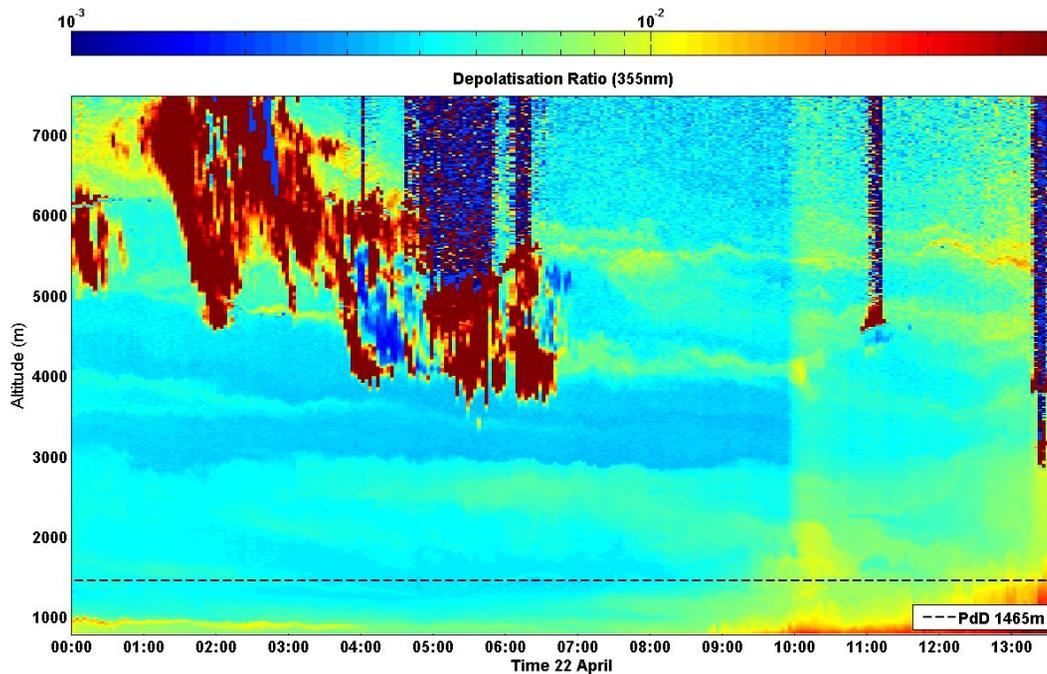
Fig. 10. LIDAR depolarisation ratio on 22 April 00:00 to 13:30 UTC.
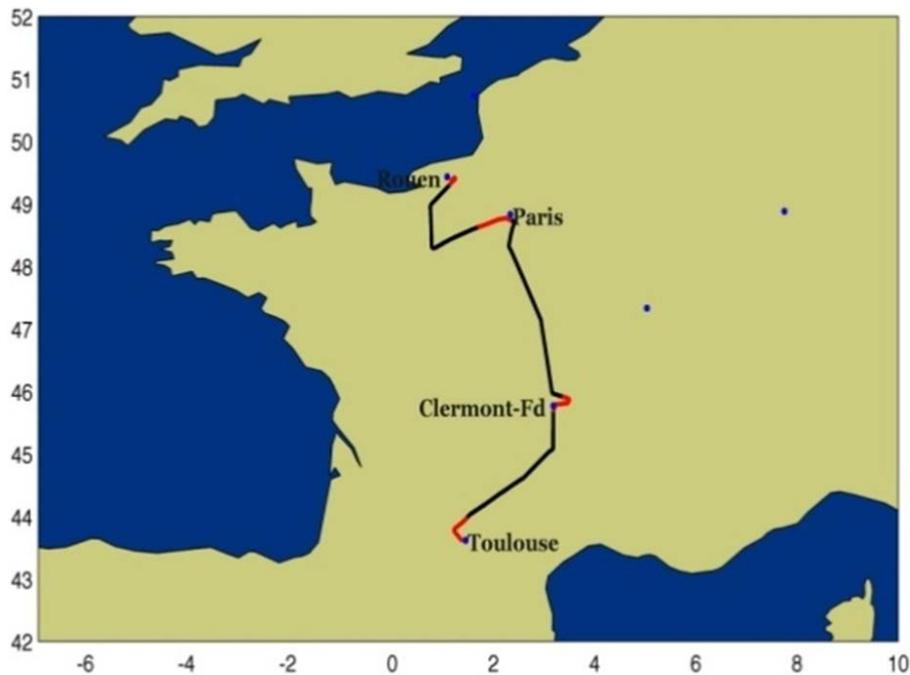
**Fig. 11.** ATR-42 trajectory on 22 April. Boundary layer measurement periods are highlighted in red.
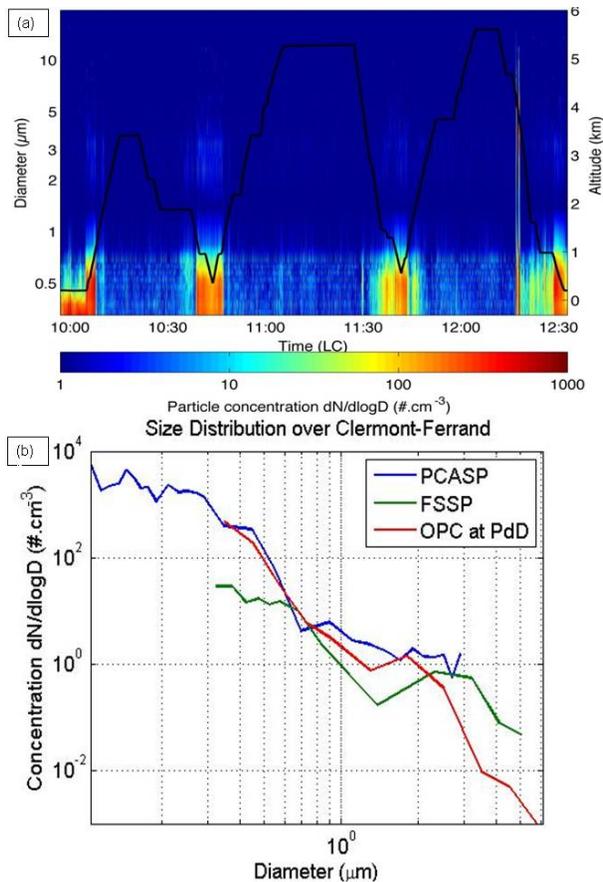
Fig. 12. Aircraft measurements on 22 April. Panel **(a)** presents the FSSP aerosol size distributions as a function of time. Particle number concentrations are colour-coded and the flight altitude is added in black. Panel **(b)** shows the mean aerosol size distributions in the PBL of Clermont-Ferrand measured during the overpass by the PCASP (in blue) and the FSSP (in green) and the ground-based OPC (in red).
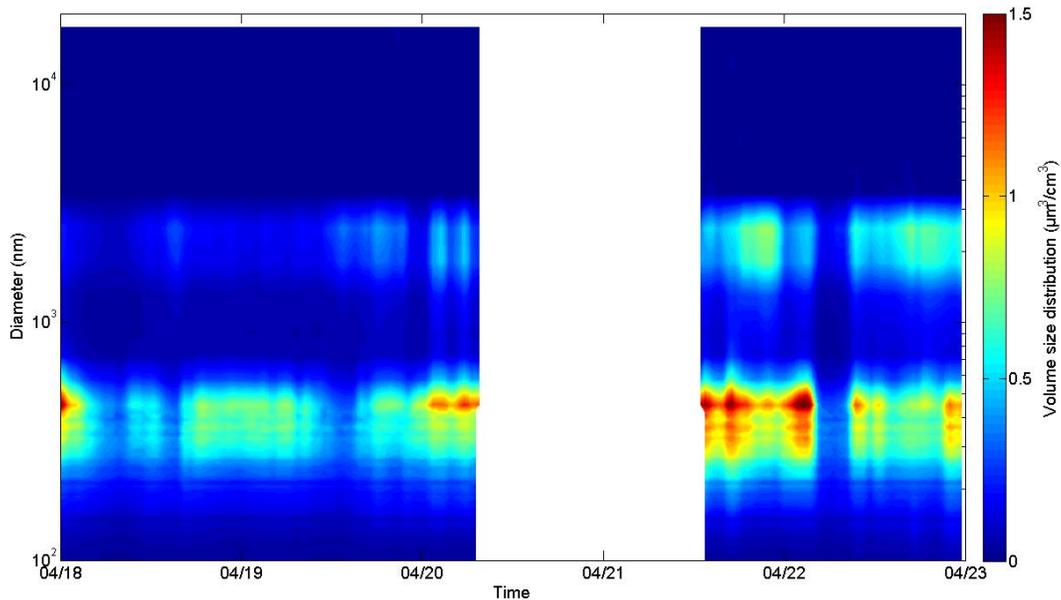
Fig. 13. Particle volume size distribution measured by a SMPS and Grimm OPC on 18–22 April 2010 at the Puy de Dôme.